






Red Spiral Galaxies at Cosmic Noon Unveiled in the First JWST Image

Yoshinobu Fudamoto^{1,2} , Akio K. Inoue^{1,3} , and Yuma Sugahara^{1,2} ¹ Waseda Research Institute for Science and Engineering, Faculty of Science and Engineering, Waseda University, 3-4-1 Okubo, Shinjuku, Tokyo 169-8555, Japan² National Astronomical Observatory of Japan, 2-21-1, Osawa, Mitaka, Tokyo, Japan³ Department of Physics, School of Advanced Science and Engineering, Faculty of Science and Engineering, Waseda University, 3-4-1, Okubo, Shinjuku, Tokyo 169-8555, Japan

Received 2022 July 29; revised 2022 October 4; accepted 2022 October 6; published 2022 October 21

Abstract

In the first image of the James Webb Space Telescope (JWST) of SMACS J0723.3-7327, one of the most outstanding features is the emergence of a large number of red spiral galaxies, because such red spiral galaxies are only a few percent in the number fraction among nearby spiral galaxies. While these apparently red galaxies were already detected with the Spitzer Space Telescope at $\sim 3\text{--}4\ \mu\text{m}$, the revolutionized view from the JWST's unprecedented spatial resolution has unveiled their hidden spiral morphology for the first time. Within the red spiral galaxies, we focus on the two reddest galaxies that are very faint in the $< 0.9\ \mu\text{m}$ bands and show red colors in the $2\text{--}4\ \mu\text{m}$ bands. Our study finds that the two extremely red spiral galaxies are likely to be in the cosmic noon ($1 < z < 3$). One of the extremely red spiral galaxies is more likely to be a passive galaxy having moderate dust reddening (i.e., \sim zero star formation rate with $A_V \sim 1$ mag). The other is consistent with both passive and dusty starburst solutions (i.e., star formation rate $> 100\ M_\odot\ \text{yr}^{-1}$ with $A_V \sim 3$ mag). These “red spiral” galaxies would be an interesting, potentially new population of galaxies, as we start to see their detailed morphology using the JWST, for the first time.

Unified Astronomy Thesaurus concepts: [Spiral galaxies \(1560\)](#); [Galaxy structure \(622\)](#); [Galaxy formation \(595\)](#); [Galaxy evolution \(594\)](#); [Galaxy stellar disks \(1594\)](#)

1. Introduction

The spiral structure of galaxies is not only one of the most spectacular features of the universe but also provides us with important information on galaxy formation and evolution. Since the first systematic classification of the morphology of “extragalactic nebulae” (Hubble 1926), large efforts have been devoted to studying the morphology of galaxies across cosmic time and to understanding their formation mechanisms (see Conselice 2014 for a review). However, when and how the galaxy morphology emerged in the early universe is still largely unknown.

Spiral galaxies typically show blue colors in their rest-frame optical wavelength and are, in general, classified as “normal” star-forming galaxies (e.g., Schawinski et al. 2014). Red or passive (i.e., non-star-forming or “anemic”; van den Bergh 1976) spiral galaxies are, on the other hand, a very minor population in the nearby universe. In the latest study, Shimakawa et al. (2022) identified nearly a thousand red, passive spiral galaxies among $\sim 55,000$ galaxies at $0.01 < z < 0.3$ from $1000\ \text{deg}^2$ imaging data obtained with the Subaru/Hyper Suprime-Cam. Hence, the fraction of the red spiral galaxies is only $\sim 2\%$ in the local universe.

It was, for the first look, surprising to find many apparently red spiral galaxies in the James Webb Space Telescope (JWST) image of the galaxy cluster, SMACS J0723.3-7327, which was released on 2022 July 11 as part of the early release observations (EROs; Pontoppidan et al. 2022). Their redness could indicate several important properties of these spiral galaxies: their dominant stellar ages, dust reddenings, or a combination of these features. Because the released image was taken by the Near Infrared Camera


(NIRCam) on the JWST over the wavelength range of $0.9\text{--}4.4\ \mu\text{m}$, the redness in NIR may indicate that these spiral galaxies are at high redshift.

Spiral galaxies in the distant universe are a very important population to examine the emergence of the spiral structure in galaxies. The most distant spiral galaxy known so far is a gas-rich galaxy, BRI 1335–0417, at $z = 4.41$ (Tsukui & Iguuchi 2021). A grand-design spiral structure traced by the [C II] line was revealed with the Atacama Large Millimeter/submillimeter Array (ALMA); however, the stellar structure of BRI 1335–0417 is still unknown. The most distant, spiral stellar disk galaxies are reported at $z = 2\text{--}3$ (Dawson et al. 2003; Law et al. 2012; Margalef-Bentabol et al. 2022; Wu et al. 2022). Searching for such galaxies at even higher redshift is the key to knowing when the stellar spiral disks emerged.

To characterize red spiral galaxies found in the JWST's ERO data, we carefully select the most extreme red spiral galaxies and examine their spectral energy distribution (SED), as a first case study. This Letter is organized as follows: In Section 2, we describe the data and the sample used in this study. In Section 3, we present our analysis. Section 4 shows the results and discussion on the red spiral galaxies found in the JWST images. We conclude in Section 5. Throughout this Letter, we assume a cosmology with $(\Omega_m, \Omega_\Lambda, h) = (0.3, 0.7, 0.7)$.

2. Data

The following images of the Hubble Space Telescope (HST) and the JWST are based on a “first-pass” reduction of the HST and JWST images of the SMACS 0723 lensing cluster field. All images have been processed with the *grizli*⁴ software pipeline. Further documentation will be provided by G. Brammer et al. (2022, in preparation).

 Original content from this work may be used under the terms of the [Creative Commons Attribution 4.0 licence](#). Any further distribution of this work must maintain attribution to the author(s) and the title of the work, journal citation and DOI.

⁴ <https://github.com/gbrammer/grizli>

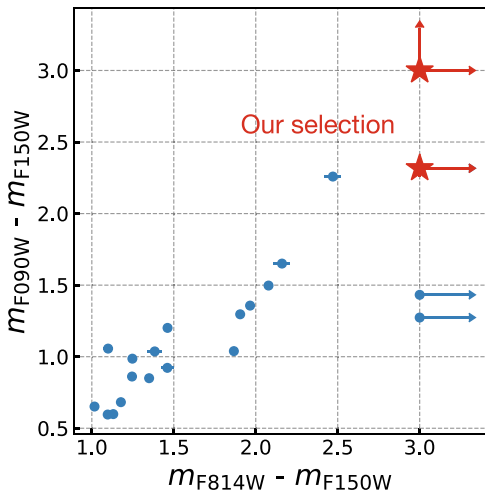


Figure 1. The observed colors of red spiral galaxies. After our visual selections of red spiral galaxies, we further down-selected the most $\sim 1\text{--}2\ \mu\text{m}$ red galaxies, which we focus on in this study (red stars). These galaxies have extremely red colors of $m_{F814W/F090W} - m_{F150W} > 2.5$ mag. Other red spiral galaxies (blue points) have at least one $>3\sigma$ detection in the HST ACS bands. We applied zero-point corrections for the JWST’s fluxes based on Adams et al. (2022).

2.1. HST Data

As part of the reionization lensing cluster survey (RELICS; Coe et al. 2019), optical and NIR images were obtained using HST. These HST images include data from Advance Camera for Surveys (ACS; F435W, F606W, F814W filters) and WFC3/IR (F105W, F125W, F140W, F160W filters) instruments. All HST data were calibrated and mosaiced in a standard manner. Final images have a pixel scale of $0''.04\ \text{pixel}^{-1}$.

2.2. JWST Data

We used JWST NIRCам images of six filters in total (F090W, F150W, F200W, F277W, F356W, and F444W). After the reprocessing of the JWST’s public data available in the MAST data archive, the final mosaic has $0''.02\ \text{pixel}^{-1}$ for the short wavelength filters (F090W, F150W, F200W), and $0''.04\ \text{pixel}^{-1}$ for the long wavelength filters (F277W, F356W, F444W). A small astrometric offset ($\sim 0''.2$) exists between HST and JWST images. The offset, however, did not affect our analysis as we manually corrected positions of apertures during our photometry.

3. Analysis

3.1. Selecting Red Spiral Galaxies

We first visually selected bright red spiral galaxies from the false-color image presented within the ERO release.⁵ Two authors (Y.F. and A.K.I.) visually selected red spiral galaxies from the image independently. We selected 21 galaxies that both agreed with having spiral structures with apparently red colors. While quantitative evaluation of galaxy types would also be preferred (e.g., Dominguez Sanchez et al. 2018; Ferreira et al. 2022), visual selections are also known to be effective and widely used, especially when finding apparent structures, such as spiral shape (e.g., Galaxy Zoo Project; Lintott et al. 2008).

To find the reddest spiral galaxies, we further down-selected samples based on their faintness in $\leq 0.9\ \mu\text{m}$ images (see

Section 3.2.1 below for the photometry of our sample here). In particular, we selected galaxies that are nondetected in the HST F814W image and, at the same time, galaxies that have an extremely red color in the F090W versus F150W image (Figure 1).

The selected red spiral galaxies (RS 13 and RS 14) were already detected by HST WFC3 and Spitzer IRAC images; however, the angular resolution of these previous instruments did not allow us to study the detailed morphology. We can now access the resolved morphology of the red spiral galaxies by the JWST’s unprecedented spatial resolution and sensitivity in these NIR wavelengths (Figure 2).

3.2. Photometry

3.2.1. HST and JWST Photometry

To measure galaxy-wide integrated fluxes, we performed aperture photometry of both HST and JWST images for the red spiral galaxies. We used python package `photutils` (Bradley et al. 2020) using elliptical apertures. We applied apertures large enough to enclose entire galaxies in the JWST F444W image to obtain integrated fluxes. Measured flux errors incorporated background noises by scaling pixel-by-pixel rms’s to aperture sizes, and Poisson noises of measured fluxes.

3.2.2. JWST Photometric Uncertainty

As calibrations of NIRCам data progressed, studies reported that the NIRCам’s photometric zero-points have uncertainties, which could be up to $\sim 20\%$ different from the preflight measurements (Adams et al. 2022; Morishita & Stiavelli 2022; Rigby et al. 2022) and/or could be time variable (Nardiello et al. 2022). In this study, we use the photometric zero-point of JWST NIRCам data based on Adams et al. (2022), which is derived using updated JWST calibration references for the SMACS 0723 field using in-flight data. These updated zero-points were, however, based on preliminary calibrations of the JWST. Therefore, further uncertainties could still be expected. To incorporate such uncertainties, we additionally applied 10% of flux uncertainties for all measured fluxes from the JWST. These uncertainties were added quadratically to the measured aperture flux errors. Additionally, we tested the effect of changing photometric zero-points in the following discussions, including values derived from in-flight throughput in Rigby et al. (2022) and the original preflight values.

3.2.3. RS 14

Within the extremely red spiral galaxies, RS 14 has already been studied in several papers. In particular, Sun et al. (2022) reported ALMA continuum detection in a $1.1\ \text{mm}$ image obtained among the ALMA large program, ALCS: 2018.1.00035.L (PI: K. Kohno). Most recently, Cheng et al. (2022) presented a joint JWST–ALMA study of this source. Also, Carnall et al. (2022) reported spectroscopic redshift of $z_{\text{spec}} = 2.463$ determined by multiple emission lines such as $\text{H}\alpha$, $[\text{N II}]$, and $[\text{S II}]$ (ID 9239 of NIRSspec spectroscopy as part of the same JWST ERO). In the following analysis, we used the ALMA continuum flux and the NIRSspec redshift for RS 14.

3.3. Lensing Magnification

We estimated gravitational lensing magnification based on the recent work by Golubchik et al. (2022). Their lens model is constructed with the `Light-Traces-Mass` method (e.g.,

⁵ <https://stsci-opo.org/STScI-01G7DDBW5NNXTJV8PGHB0465QP.png>

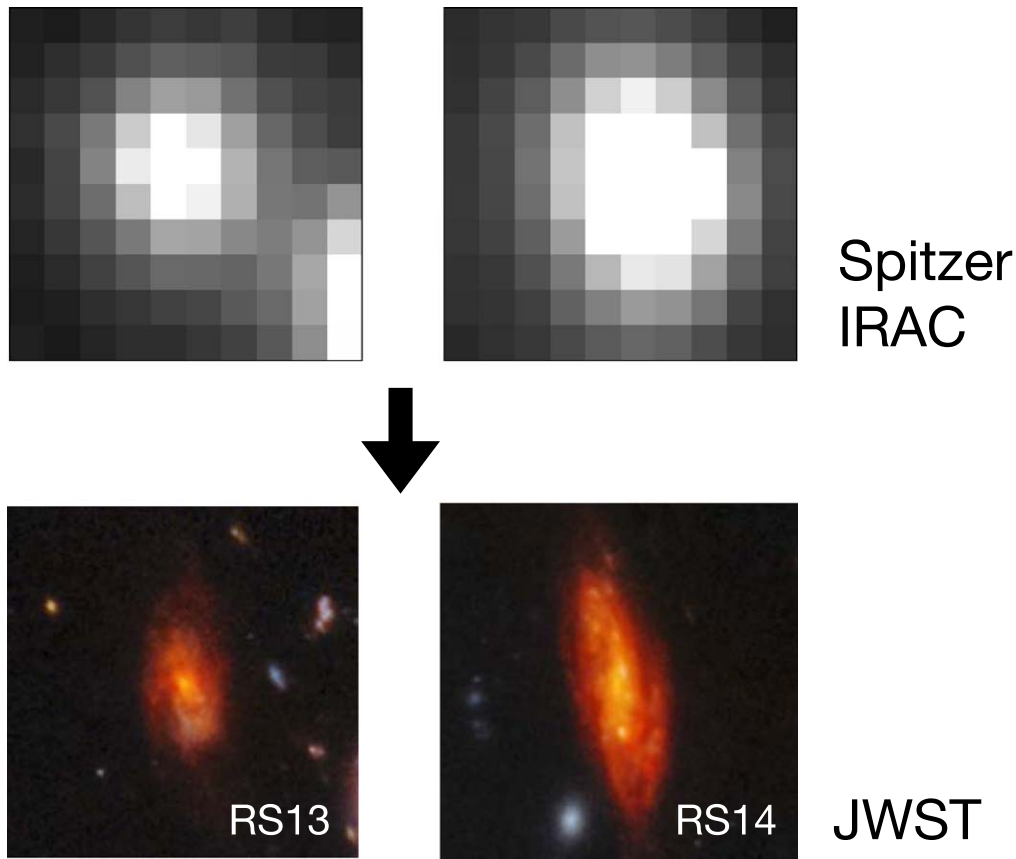


Figure 2. Demonstrations of the improved spatial resolution by JWST observations: (Upper panels) Spitzer IRAC $3.6 \mu\text{m}$ images of the extremely red spiral galaxies in the SMACS 0723 field. (Lower panels) false-color images by the JWST’s F090W, F150W, F200W, F277W, F356W, and F444W filters. All images have spatial scales of $5'' \times 5''$. The arm and bulge structure of the galaxies are captured for the first time, thanks to the extremely high resolution and sensitivity of the JWST. North is up and east is left for both Spitzer IRAC and JWST images. Copyright: NASA/STScI.

Broadhurst et al. 2005), which infers the lens mass contributions from the cluster’s light distributions, using HST and Very Large Telescope MUSE data. We estimated lensing magnification factors by assuming redshifts from the following SED fittings.

3.4. Spectral Energy Distribution Fittings

To constrain the physical properties and redshift of RS 13, one of our extremely red spiral galaxies, we used SED fitting code PANHIT (Mawatari et al. 2020). We assumed a Chabrier initial mass function in a range of $0.1\text{--}100 M_{\odot}$ (Chabrier 2003), the BC03 stellar population model (Bruzual & Charlot 2003), a nebular continuum and line emission model (Inoue 2011), and a standard dust attenuation curve (Calzetti et al. 2000). The star formation history is assumed to be the “delayed- τ ” model (Speagle et al. 2014) to describe a variety of star formation histories, and the star formation timescale τ_{SF} is a free parameter between 0.01 and 10 Gyr. We allowed for metallicities ranging from $0.005 \times Z_{\odot}$ to $2.5 \times Z_{\odot}$, where the solar metallicity of $Z_{\odot} = 0.02$. The dust attenuation in the V band (A_V) is also a free parameter. The age of the stellar population is another free parameter between 1 Myr and 15 Gyr, and the cosmic age limits the age at the redshift of interest. For RS 13, the redshift is another free parameter and we examined redshifts from 0.1 to 13.0 with a step of 0.1. The stellar mass and star formation rate (SFR) were determined by scaling the amplitude of the SED. The SED fits performed the χ^2 minimization algorithm for the photometry data, including the nondetection bands (i.e., upper limits; Sawicki 2012).

Additionally, to test the robustness of our SED fittings, we also used the SMC dust extinction curve (Gordon et al. 2003) as well as assuming constant and then truncated star formation history.

For RS 14, we run the fitting with the spectroscopic redshift of $z = 2.463$ (Carnall et al. 2022) and including the ALMA continuum flux (Cheng et al. 2022). PANHIT assumes energy conservation between the stellar radiation absorbed by dust and the far-infrared (FIR) emission from dust. We assumed modified blackbody functions with an emissivity index $\beta = 2$ and the dust temperature, T_d , between 10 and 50 K with a step of 5 K. Note that the cosmic microwave background temperature at $z = 2.463$ is 9.5 K, a strict lower limit of T_d .

4. Results and Discussion

4.1. SED Fitting Results

We found that the redshifts of extremely red spirals are in a range of $z_{\text{ph}} = 1\text{--}3$. In particular, RS 14 ($z_{\text{spec}} = 2.463$) is one of the highest redshift spiral galaxies identified so far (Dawson et al. 2003; Law et al. 2012; Margalef-Bentabol et al. 2022; Wu et al. 2022).

Our SED fits showed that two types of integrated properties exist for the extremely red spiral galaxies at $1 < z < 3$: (1) old stellar populations that are consistent with almost completely passive, non-star-forming galaxies, or (2) dust-obscured highly elevated star formation activities. In our SED fits, these properties are indicated from the JWST’s coverage of $\lambda_{\text{rest}} \sim 4300\text{--}12,800 \text{ \AA}$ photometry. The red colors of these bands can be explained

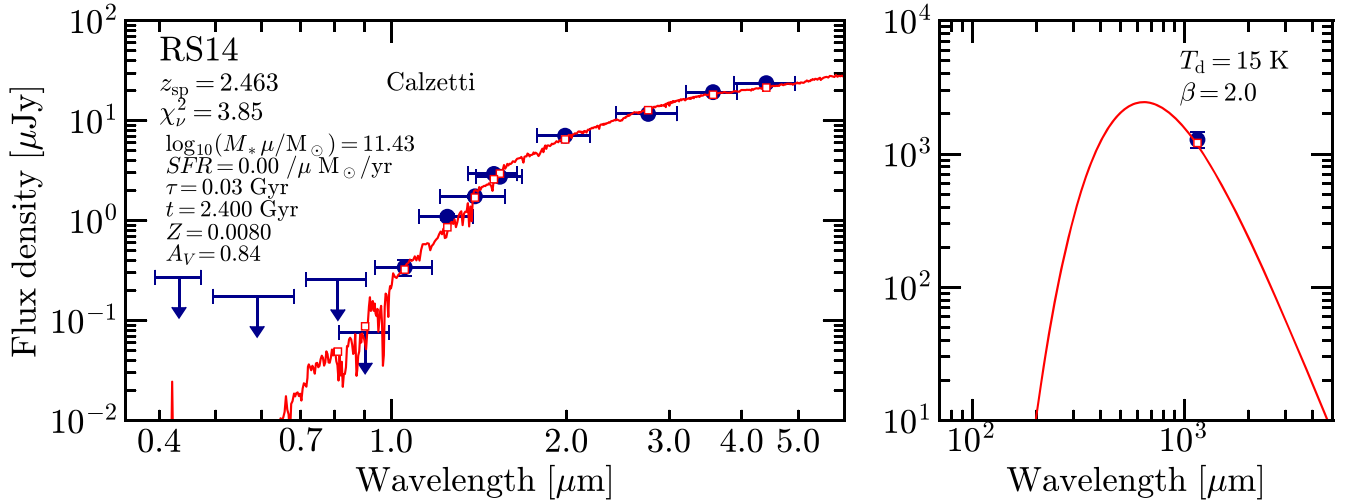


Figure 3. The best-fit SED of RS 14 derived by fixing its redshift at $z_{\text{sp}} = 2.463$. Integrated JWST photometry can be represented solely by old stellar populations, thus not requiring considerable dust reddening and star formation. The SED fitting results indicate that RS 14 represents a passive spiral galaxy at high redshift.

Table 1

A Summary of SED Fitting Results and Lensing Magnification Factors

RS 13	Best Fit	Second Best
z_{ph}	2.2 ± 0.1	$2.8^{+0.1}_{-0.2}$
χ^2_{ν}	1.25	1.54
$\log_{10}(M_* \times \mu [M_{\odot}])$	$9.95^{+0.07}_{-0.01}$	$10.45^{+0.04}_{-0.01}$
$SFR \times \mu (M_{\odot} \text{ yr}^{-1})$	450 ± 170	$0.17^{+0.01}_{-0.17}$
A_V (mag)	$3.07^{+0.06}_{-0.07}$	$0.59^{+0.13}_{-0.20}$
Age (Gyr)	$0.020^{+0.025}_{-0.002}$	$0.36^{+0.13}_{-0.09}$
τ_{SF} (Gyr)	0.01–10	$0.03^{+0.01}_{-0.02}$
Z	0.03–0.06	0.03–0.05
μ	1.67 ± 0.02	1.75 ± 0.03
<hr/>		
RS 14		
z_{sp}	2.463	
χ^2_{ν}	3.84	
$\log_{10}(M_* \times \mu [M_{\odot}])$	11.43 ± 0.03	
$SFR \times \mu (M_{\odot} \text{ yr}^{-1})$	0.00	
A_V (mag)	$0.84^{+0.12}_{-0.03}$	
Age (Gyr)	$2.4^{+0.1}_{-0.2}$	
τ_{SF} (Gyr)	0.03–0.1	
Z	0.007–0.012	
T_{dust} (K)	~ 15	
μ	2.16 ± 0.06	

by old stellar populations with moderate dust attenuation, or dust-obscured star formation activity. In particular, the possibility of populations of red and dead spiral galaxies at $z > 1$ in our extremely red spiral sample is very interesting, as they are very rare in the local universe (Shimakawa et al. 2022).

We note that our SED fit results could have some caveats, such as uncertain calibration of JWST photometry, which would change observed colors of these galaxies (see also Morishita & Stiavelli 2022 for different photometric zero-point corrections). Also, the physical properties of these red spiral galaxies are not well studied yet. Thus, other assumptions that are not included in our SED fits could be allowed, such as a much steeper dust attenuation curve. However, we test several reasonable cases to incorporate these possible caveats. As a result, we always find that the extremely red spiral galaxies show photometric redshift

$z \sim 1\text{--}3$ and have passive stellar populations or dust-obscured star formation activities. In particular, RS 14 always shows a passive stellar population even if we use several photometric zero-points or assumptions for SED fits.

Table 1 is a summary of the fitting results as well as the lensing magnification factors. Following this, we describe the results of our SED fitting in detail.

4.1.1. RS 14

We found that the $T_{\text{d}} = 15$ K case delivered the minimum χ^2 value compared to other T_{d} cases. Higher T_{d} with fixing 1.1 mm flux leads to larger IR luminosity, and thus, larger dust attenuation; however, it makes the rest-frame optical SED traced by NIRCcam too red. As such, the $T_{\text{d}} = 15$ K, rather low temperature (e.g., Schreiber et al. 2018), seems the best representation for RS 14, which is shown in Figure 3.

The best-fit model for RS 14 consists of a passive, old stellar population, and moderate dust attenuation ($A_V = 0.84^{+0.12}_{-0.03}$). The age is much longer than the star formation timescale, $\tau_{\text{SF}} \lesssim 0.1$ Gyr, and the current SFR is almost zero. This feature supports the very low T_{d} (15 K) that is heated by old stars rather than massive young stars. The stellar mass is relatively high, $1.0 \times 10^{11} M_{\odot}$ after correcting a magnification of $\mu = 2.16$ at $z_{\text{spec}} = 2.463$.

The best-fit passive solution of RS 14 does not change if we use different photometric zero-points, including the preflight value, or if we use different assumptions for the SED fitting. In particular, we also applied a steeper dust attenuation (i.e., the one from the SMC dust extinction curve; Gordon et al. 2003). However, the results do not change.

While the galaxy-wide integrated property of RS 14 is consistent with a non-star-forming passive galaxy, the JWST's F090W image (the rest-frame wavelength of ~ 2600 Å) shows a few faint clumps in the bulge and some parts of the spiral arm region of RS 14, which is smoothed out by our photometry using a large aperture. As these clumps can be seen in the rest-frame UV wavelength, a small amount of star formation activity is still ongoing in RS 14. This is also consistent with the H α emission line detection (Carnall et al. 2022). Hence, RS 14 may have small but substantial star formation activity.

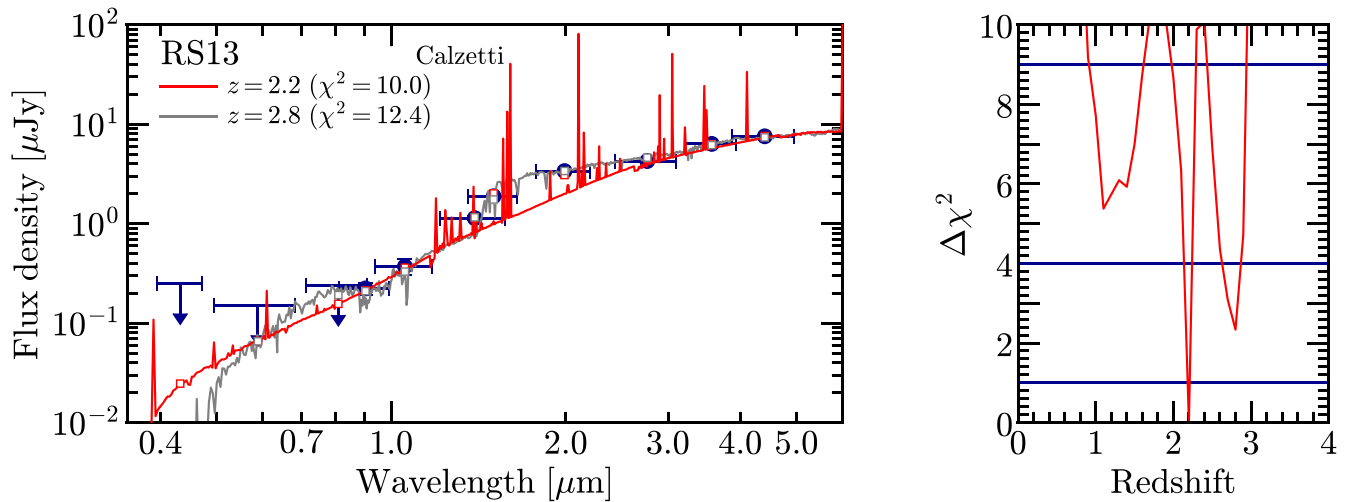


Figure 4. SED fitting results of RS 13: left panel shows the SEDs inferred from our fitting. Right panel shows reduced χ^2_{ν} as a function of redshift. For RS 13, photometric redshift is loosely constrained at $1 < z < 3$. The best fit is a dusty star-forming solution at $z_{\text{ph}} = 2.2 \pm 0.1$ (red solid line in the left panel), and the second best fit is a passive solution with $\text{SFR} \sim 0$ at $z_{\text{ph}} = 2.8^{+0.1}_{-0.2}$ (gray solid line in the left panel).

4.1.2. RS 13

For RS 13, we found a global χ^2 minimum in the redshift range of $1 \lesssim z \lesssim 3$ (lower right panel of Figure 4), showing two local minima at $z = 2.2$ and $z = 2.8$.

The best redshift solution of RS 13 is $z_{\text{ph}} = 2.2 \pm 0.1$, having a large dust reddening of $A_V = 3.07^{+0.06}_{-0.07}$ with a high SFR of $\sim 450 M_{\odot} \text{yr}^{-1}$. This solution explains that some of the $>1 \mu\text{m}$ fluxes seen in NIRCcam bands are produced by strong optical-to-NIR nebular lines, instead of the stellar continuum. With the young age of 0.02 Gyr, this solution suggests that RS 13 is a dusty starburst spiral galaxy.

Another redshift solution is $z_{\text{ph}} = 2.8^{+0.1}_{-0.2}$. For this solution, RS 13 is similar to RS 14, a passive galaxy (SFR consistent with zero) with the stellar age of 0.4 Gyr, showing the clear Balmer break around F140W and F150W filter wavelengths. The stellar mass is $\sim 2 \times 10^{10} M_{\odot}$ after correcting a magnification.

Although these two solutions show largely different properties for RS 13, both solutions show that the redshift of RS 13 is $1 < z < 3$. These general results do not change if we use different photometric zero-points or different assumptions for SED fittings. Further disentangling these two possible properties (i.e., a dusty starburst spiral or a passive spiral) requires spectroscopic redshift.

5. Conclusion

In this Letter, we studied the properties of two extremely red spiral galaxies (RS 13 and RS 14) found from the JWST ERO image data release of SMACS 0723. These extremely red spiral galaxies are among a sample of red spiral galaxies visually selected from the ERO data. By performing SED fitting to these extremely red spiral galaxies, we found the following results:

1. Most likely redshifts of the extremely red spirals are $1 < z < 3$, i.e., in the cosmic noon. The results show that these red spiral galaxies in JWST images contain the most distant spiral galaxies known to date. Within them, RS 14 is currently one of the most distant stellar spiral galaxies, having $z_{\text{spec}} = 2.463$.
2. Our SED fits suggest that the extremely red spiral galaxies are passive galaxies or heavily dust-obscured galaxies. These

properties are indicated from the red colors of the rest-frame wavelength of $\sim 4300\text{--}12,800 \text{ \AA}$ in the JWST photometry.

3. One of the extremely red spiral galaxies, RS 14, is found to be a passive spiral galaxy. Finding passive spiral galaxies in the early universe is surprising, as most of the spiral galaxies found in the local universe are young star-forming galaxies.

Further detailed studies would be required to understand the formation mechanisms and evolutionary path of the red spiral galaxies. Follow-up observations using integral field spectroscopy, including high-resolution ALMA observations, will provide kinematics, molecular gas, and dust distribution of high-redshift spiral galaxies.

We thank Ken Mawatari for helpful comments and discussions for SED fittings. We also thank Fengwu Sun, Ryosuke Uematsu, and Marc Postman for very helpful discussions. Y.F., A.K.I., and Y.S. acknowledge support from NAOJ ALMA Scientific Research grant No. 2020-16B. The Early Release Observations and associated materials were developed, executed, and compiled by the ERO production team: Hannah Braun, Claire Blome, Matthew Brown, Margaret Carruthers, Dan Coe, Joseph DePasquale, Nestor Espinoza, Macarena Garcia Marin, Karl Gordon, Alaina Henry, Leah Hustak, Andi James, Ann Jenkins, Anton Koekemoer, Stephanie LaMassa, David Law, Alexandra Lockwood, Amaya Moro-Martin, Susan Mullally, Alyssa Pagan, Dani Player, Klaus Pontoppidan, Charles Proffitt, Christine Pulliam, Leah Ramsay, Swara Ravindranath, Neill Reid, Massimo Robberto, Elena Sabbi, Leonardo Ubeda. The EROs were also made possible by the foundational efforts and support from the JWST instruments, STScI planning and scheduling, and Data Management teams. All the JWST data used in this Letter can be found in MAST: [10.17909/hqs6-qy97](https://doi.org/10.17909/hqs6-qy97).

Facilities: HST, JWST (STIS).

Software: astropy (Astropy Collaboration et al. 2013, 2018), photutils (Bradley et al. 2020), PANHIT (Mawatari et al. 2020).

ORCID iDs

Yoshinobu Fudamoto <https://orcid.org/0000-0001-7440-8832>
 Akio K. Inoue <https://orcid.org/0000-0002-7779-8677>
 Yuma Sugahara <https://orcid.org/0000-0001-6958-7856>

References

- Adams, N. J., Conselice, C. J., Ferreira, L., et al. 2022, arXiv:2207.11217
- Astropy Collaboration, Robitaille, T. P., Tollerud, E. J., et al. 2013, *A&A*, **558**, A33
- Astropy Collaboration, Price-Whelan, A. M., Sipőcz, B. M., et al. 2018, *AJ*, **156**, 123
- Bradley, L., Sipocz, B., Robitaille, T., et al. 2020, astropy/photutils: v1.0.0, Zenodo, doi:10.5281/zenodo.4044744
- Broadhurst, T., Benítez, N., Coe, D., et al. 2005, *ApJ*, **621**, 53
- Bruzual, G., & Charlot, S. 2003, *MNRAS*, **344**, 1000
- Calzetti, D., Armus, L., Bohlin, R. C., et al. 2000, *ApJ*, **533**, 682
- Carnall, A. C., Begley, R., McLeod, D. J., et al. 2022, arXiv:2207.08778
- Chabrier, G. 2003, *PASP*, **115**, 763
- Cheng, C., Yan, H., Huang, J.-S., et al. 2022, *ApJL*, **936**, L19
- Coe, D., Salmon, B., Bradač, M., et al. 2019, *ApJ*, **884**, 85
- Conselice, C. J. 2014, *ARA&A*, **52**, 291
- Dawson, S., McCrady, N., Stern, D., et al. 2003, *AJ*, **125**, 1236
- Dominguez Sanchez, H., Huertas-Company, M., Bernardi, M., Tuccillo, D., & Fischer, J. L. 2018, *MNRAS*, **476**, 3661
- Ferreira, L., Adams, N., Conselice, C. J., et al. 2022, arXiv:2207.09428
- Golubchik, M., Furtak, L. J., Meena, A. K., & Zitrin, A. 2022, arXiv:2207.05007
- Gordon, K. D., Clayton, G. C., Misselt, K. A., Landolt, A. U., & Wolff, M. J. 2003, *ApJ*, **594**, 279
- Hubble, E. P. 1926, *ApJ*, **64**, 321
- Inoue, A. K. 2011, *MNRAS*, **415**, 2920
- Law, D. R., Shapley, A. E., Steidel, C. C., et al. 2012, *Natur*, **487**, 338
- Lintott, C. J., Schawinski, K., Slosar, A., et al. 2008, *MNRAS*, **389**, 1179
- Margalef-Bentabol, B., Conselice, C. J., Haeussler, B., et al. 2022, *MNRAS*, **511**, 1502
- Mawatari, K., Inoue, A. K., Yamanaka, S., Hashimoto, T., & Tamura, Y. 2020, in IAU Symp. 341, Challenges in Panchromatic Modelling with Next Generation Facilities, ed. M. Boquien et al. (Cambridge: Cambridge Univ. Press), 285
- Morishita, T., & Stiavelli, M. 2022, arXiv:2207.11671
- Nardiello, D., Bedin, L. R., Burgasser, A., et al. 2022, *MNRAS*, **517**, 484
- Pontoppidan, K., Blome, C., Braun, H., et al. 2022, *ApJL*, **936**, L14
- Rigby, J., Perrin, M., McElwain, M., et al. 2022, arXiv:2207.05632
- Sawicki, M. 2012, *PASP*, **124**, 1208
- Schawinski, K., Urry, C. M., Simmons, B. D., et al. 2014, *MNRAS*, **440**, 889
- Schreiber, C., Elbaz, D., Pannella, M., et al. 2018, *A&A*, **609**, A30
- Shimakawa, R., Tanaka, M., Bottrell, C., et al. 2022, *PASJ*, **74**, 612
- Speagle, J. S., Steinhardt, C. L., Capak, P. L., & Silverman, J. D. 2014, *ApJS*, **214**, 15
- Sun, F., Egami, E., Fujimoto, S., et al. 2022, *ApJ*, **932**, 77
- Tsukui, T., & Iguchi, S. 2021, *Sci*, **372**, 1201
- van den Bergh, S. 1976, *ApJ*, **206**, 883
- Wu, Y., Cai, Z., Sun, F., et al. 2022, arXiv:2208.08473